

Article

Performance and Effect of Load Mitigation of a Trailing-Edge Flap in a Large-Scale Offshore Wind Turbine

Xin Cai ¹, Yazhou Wang ¹, Bofeng Xu ^{1,2,*} and Junheng Feng ¹

¹ College of Mechanics and Materials, Hohai University, Nanjing 211100, China; xcai@hhu.edu.cn (X.C.); wangyazhou@ctnei.com (Y.W.); fengjunheng0@163.com (J.F.)

² College of Energy and Electrical Engineering, Hohai University, Nanjing 211100, China

* Correspondence: bfxu1985@hhu.edu.cn

Received: 8 January 2020; Accepted: 21 January 2020; Published: 23 January 2020



Abstract: As a result of the large-scale trend of offshore wind turbines, wind shear and turbulent wind conditions cause significant fluctuations of the wind turbine's torque and thrust, which significantly affect the service life of the wind turbine gearbox and the power output stability. The use of a trailing-edge flap is proposed as a supplement to the pitch control to mitigate the load fluctuations of large-scale offshore wind turbines. A wind turbine rotor model with a trailing-edge flap is established by using the free vortex wake (FVW) model. The effects of the deflection angle of the trailing-edge flap on the load distribution of the blades and wake flow field of the offshore wind turbine are analyzed. The wind turbine load response under the control of the trailing-edge flap is obtained by simulating shear wind and turbulent wind conditions. The results show that a better control effect can be achieved in the high wind speed condition because the average angle of attack of the blade profile is small. The trailing-edge flap significantly changes the load distribution of the blade and the wake field and mitigates the low-frequency torque and thrust fluctuations of the turbine rotor under the action of wind shear and turbulent wind.

Keywords: offshore wind turbine; trailing-edge flap; load mitigation; free vortex wake

1. Introduction

Wind energy systems, especially those offshore, face difficult competition from traditional carbon-based energy sources with respect to cost competitiveness per kilowatt hour. To counter this problem, many energy systems have increased in size and power in order to achieve utility-scale production and to access higher winds aloft [1,2]. Recently, the large-scale offshore wind turbine has had more than 5 MW of the power and more than 80 m of the blade length. However, unsteady factors such as wind shear and turbulent wind have more negative effects on the stable operation of large wind turbines. The stability of the load and the output power has become significant issues in large-scale offshore wind turbines. There are many cases of fatigue failure of bearings and gearboxes prior to the end of the design life, which indicates the necessity of load mitigation control [3]. As the blade inertia of large-scale offshore machines is very large, traditional pitch control methods are unable to handle the fast-changing aerodynamic load fluctuations [4]. A new load control system has to be developed.

Investigations into the load mitigation of large wind turbines has mainly focused on two aspects. One aspect is research on advanced transmission systems [5]. The flexible coupled tower and blade [6] was investigated for the absorption of the instantaneous change in the torque and the reduction of the impact load of the gearbox and generator. An advanced hydraulic torque converter [7,8] is also an efficient transmission control structure. It absorbs the impact load caused by turbulent

wind, and accurately adjusts the speed of the output shaft; this results in efficient speed control of the permanent magnet synchronous generator unit and even cancels the frequency converter. The VESTAS Company has successfully applied hydraulic torque converters to its wind turbines. The other aspect is research on smart rotors [4]. Smart rotors control the amount of wind energy absorption by the wind turbine using flow control technology, including passive or active flow control devices, to reduce the load fluctuation of the wind turbine at the source. Smart rotors not only reduce load fluctuations but also the swing amplitude of the blade and the noise level. Active flow control equipment is an efficient control mode and with quick response to airload can be achieved in complex and unsteady conditions. Passive flow control devices are simple and stable, and can be implemented by performing only minor modifications to the existing blade structure [9]. Hansen and Madsen [10] reviewed both types of devices, including deformable trailing-edge, microtabs, morphing, active twist, synthetic jets, active vortex generators, and plasma actuators. In these flow control devices, deformable trailing-edge flaps have been investigated by many scholars due to their simple structure and considerable adjustability [11,12]. Although, trailing-edge flaps are still in the research stage, this technology is the most likely approach to be put into practical application of the large-scale blade first.

Bak et al. [13] conducted a wind tunnel test of the wind turbine airfoil Risø-B1-18 equipped with an active trailing edge flap. Steady-state and dynamic tests were performed with certain deflections of the active trailing edge flap. The steady-state tests showed that deflecting the flap towards the pressure side resulted in higher lift values and deflecting the flap towards the suction side provided lower lift values. Lee and Su [14] analyzed joint trailing-edge flaps and obtained the basic aerodynamic characteristics of two-dimensional airfoils with flaps. Lu et al. [15] examined and optimized the flexible variable camber trailing-edge flap. Lackner and Kuik [16] investigated the load reduction capabilities of trailing edge flaps of a 5 MW wind turbine. The results showed that the use of trailing-edge flaps and the proposed feedback control approach were effective in reducing the fatigue loads of the blades relative to the baseline. Xu et al. [17] studied the trailing-edge flap control of large-scale floating wind turbines and found that the trailing-edge flap exhibited excellent power fluctuation mitigation of large floating wind turbines. Recent publications indicate that there are relatively few studies on the effect of the flap motion on the load fluctuation of wind turbine blades under unsteady conditions.

In this study, the free vortex wake (FVW) method [18] is used to analyze the influence of the deflection angle of the flaps on the wind turbine blade aerodynamic load and wake flow field and is described and validated firstly. Subsequently, the aerodynamic performance of the airfoil, with the trailing-edge flap, as well as the influence of the trailing-edge flap on the blade aerodynamic load and the wake flow field, are analyzed in detail. Finally we elaborate on the trailing-edge flap control strategy, which is proposed by Xu et al. [17], used for an offshore wind turbine and the control performance under different wind conditions.

2. FVW Model and Validation

Figure 1 shows the structural model of the wind turbine. The red parts in the figure are the trailing-edge flaps. The influence of the tower on the aerodynamic performance, which is much smaller than that of unsteady wind conditions due to the upwind structure [19], is neglected in the calculation. In this study, the FVW method is used to simulate the aerodynamic performance of the wind turbine with trailing flaps. The FVW method simulates the aerodynamic characteristics of the blades by attaching vortices on 1/4 chord lines. Because the gradient of the attachment of the vortices is non-uniform, the blades are discretized into a finite number of micro-segments by using the arc-cosine method. Finally, the whole blade is simulated as a Weissinger-L model [20]. The load distribution of the blade is obtained by calculating the velocities induced by the vortices in the wake.

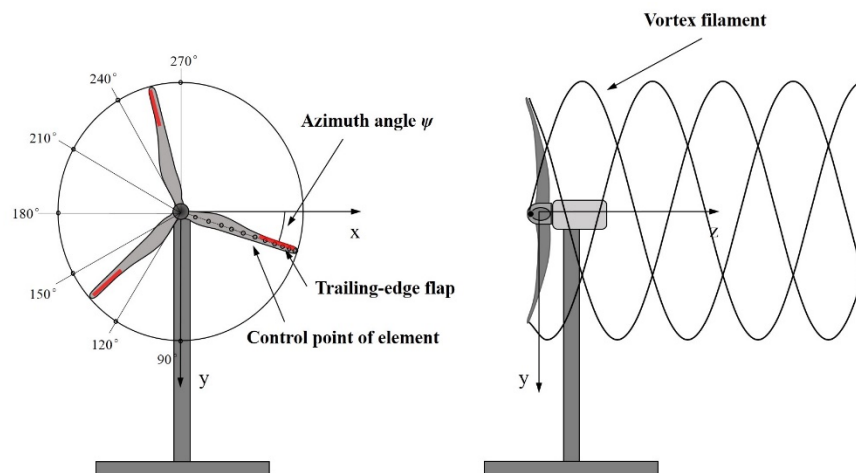


Figure 1. Wind turbine model with trailing-edge flap used in the free vortex wake (FVW) method.

The boundary of the blade element is defined by the following relationship,

$$(\bar{r})_i = \frac{(r_b)_i}{R} = \frac{2}{\pi} \cos^{-1}\left(1 - \frac{i-1}{N_E}\right) \tag{1}$$

where N_E is the number of blade elements ($N_E = 30$ in this study) and i is the element boundary number ($i = 2, \dots, N_E + 1$). Consequently, there are N_E element control points and $(N_E + 1)$ boundary points. The details of the FVW method for wind turbine aerodynamic calculations can be found in Ref. [18] and Ref. [21].

In order to verify the accuracy of the FVW method, we use it to model the NREL 5-MW wind turbine [22] and calculate the power and thrust of the rotor under stable wind conditions of 6 m/s to 18 m/s. The results are shown in Figure 2 and indicate that the calculated values (RotPwr result, RotThrust result) are close to the calculated values obtained with the FAST software (RotPwr, RotThrust) [22] at almost all wind speeds. Furthermore, some more validations of the FVW model comparing with the experimental results under the unsteady conditions including pitching case and yawed case can be found in Ref. [18]. Therefore, it is evident that the FVW model can be used to calculate the power and thrust of the wind turbine and that the calculation accuracy meets the research requirements.

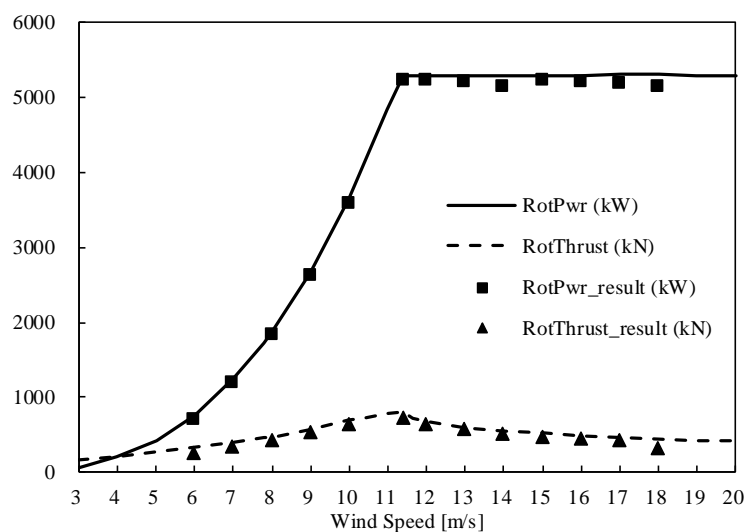


Figure 2. Power and thrust outputs of the NREL 5-MW wind turbine as a function of wind speed.

3. Aerodynamic Performance of Trailing-Edge Flap

The radial location of the trailing-edge flap should be close to the blade tip because of longer arm of force and smaller angle of attack at the outer part of the blade. Moreover, this layout can provide good control efficiency. The flap width should be appropriate to avoid damaging the blade structure. The size of the trailing-edge flaps of the NREL 5-MW wind turbine has been investigated in Ref. [17]. Here we also use the NREL 5-MW wind turbine as an example and the same size trailing-edge flaps as were described in Ref. [17], as shown in Figure 3. The flap width is 20% of the chord length; the radial flap length is 14 m in the radial direction of the blade, which is shown in red in the figure. The outboard location of the flap is 1.2 m from the blade tip. The thickness baseline of the profile with the flap was 18% and the NACA64-218 airfoil was used. The lift and drag coefficients of the NACA64-218 airfoil are calculated by the CFD (computational fluid dynamics) method [23]. The lift coefficient and lift-drag ratio of the NACA64-218 airfoil are shown in Figure 4. It is evident that the lift coefficient of the airfoil increases with the increase in the flap deflection angle at the same angle of attack. The larger the angle of attack, the larger the lift coefficient at the same flap deflection angle, but the rate of increase in the lift coefficient decreases with increasing angle of attack. It is noteworthy that when the angle of attack is greater than 8° , the lift coefficient of the airfoil does not increase or even decreases when the flap deflection angle is greater than 15° . According to the aerodynamic analysis of the trailing-edge flap by Zhang et al. [24], a stall of the trailing-edge will occur when the flap deflection angle is too large. This will result in a drop in the lift coefficient and an increase in drag. The lift-to-drag ratio of the airfoil increases first and then decreases with the increase in the flap deflection angle. The larger the angle of attack of the airfoil, the smaller the rate of increase is and the smaller the flap deflection angle of the maximum lift-drag ratio is. When the flap deflection angle is greater than 10° , the lift-to-drag ratios cease to increase or even decrease.

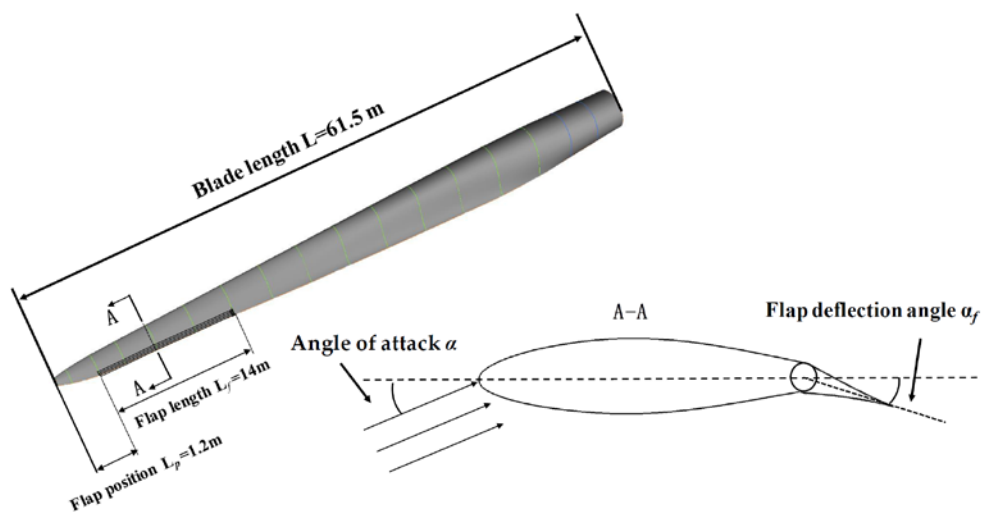


Figure 3. Blade structure with trailing-edge flap.

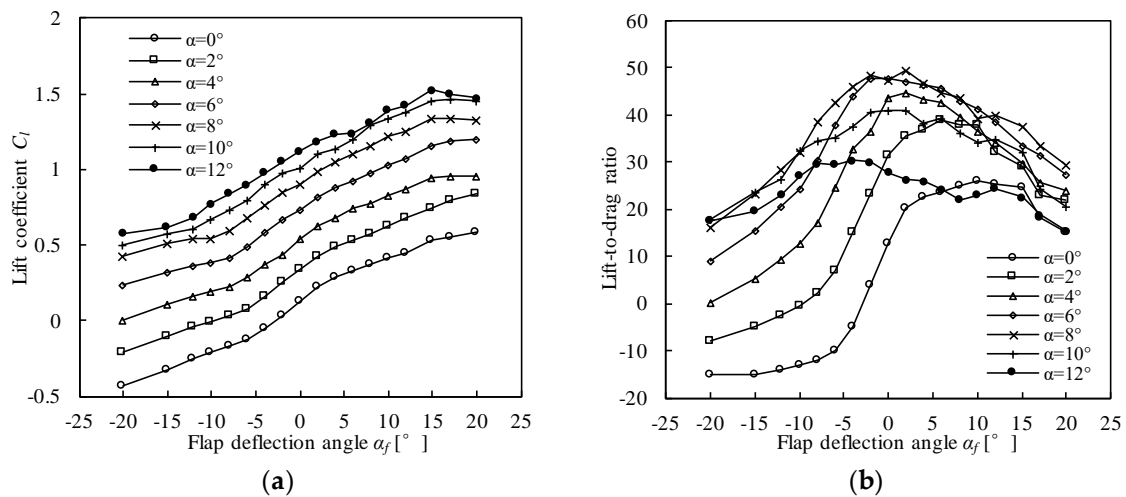


Figure 4. Aerodynamic performance of the airfoil NACA 64-218 with a trailing-edge flap. (a) Lift coefficient; (b) Lift-to-drag ratio.

4. Aerodynamic Characteristics of Trailing Flaps at Different Deflection Angles and Wind Speeds

Generally, the angle of attack has a large influence on the lift coefficient and lift-to-drag ratio of the airfoil with a flap. Therefore, it is necessary to know the angle of attack of the blade profile with the trailing-edge flap and its influence. Table 1 shows the rotor speed, blade pitch angle, and average angle of attack of the profile equipped with the trailing-edge flap of the NREL 5 MW wind turbine at different wind speeds. When the wind speed is less than the rated wind speed, the pitch angle is 0 and the rotor speed varies with the change in the wind speed. The average angle of attack of the selected profile increases slowly from 7.27° to 8.39°. When the wind speed is higher than the rated wind speed, the pitch angle increases, whereas the speed of the rotor does not change and the average angle of attack of the selected profile decreases gradually. As seen in Figure 4, the effect of the flap deflection angle on the aerodynamic performance differs for different angles of attack. Therefore, the effect of the flap deflection angle on the aerodynamic performance of the blade has to be determined.

Table 1. Rotor speed, blade pitch angle, and average angle of attack of the profile with the trailing-edge flap at different wind speeds.

Wind Speed (m/s)	Rotor Speed (rpm)	Pitch Angle (°)	Average Angle of Attack (°)
8	9.16	0.00	7.27
9	10.37	0.00	7.60
10	11.48	0.00	7.69
11.4	12.1	0.00	8.39
12	12.1	3.83	5.07
14	12.1	8.70	1.91
16	12.1	12.06	0.28
18	12.1	14.92	-0.85

The wind turbine torque and thrust for different flap deflection angles at three stable wind speeds of 8 m/s, 11.4 m/s, and 16 m/s are shown in Figure 5. The trends of the torque curves are similar at 8 m/s and 11.4 m/s. In the flap deflection angle range of -20° – 0° , the torque increases with the increase in the flap deflection angle but it only increases slightly in the range of 0° – 5° and even decreases in the range of 5° – 10° . The torque values at 16 m/s increase in the range of -20° – 10° and the slope of the curve decreases only when approaching 10° . The thrust curves are also similar at 8 m/s and 11.4 m/s. When the flap deflection angle is greater than 0° , the rate of increase in the thrust values is relatively small at these wind speeds, whereas the rate of increase in the thrust values at 16 m/s is greater. The

control performance of the flap is related to the angle of attack of the profile. At high wind speeds, the smaller the angle of attack of the profile, the better the control performance is; this result is consistent with the results shown in Figure 4.

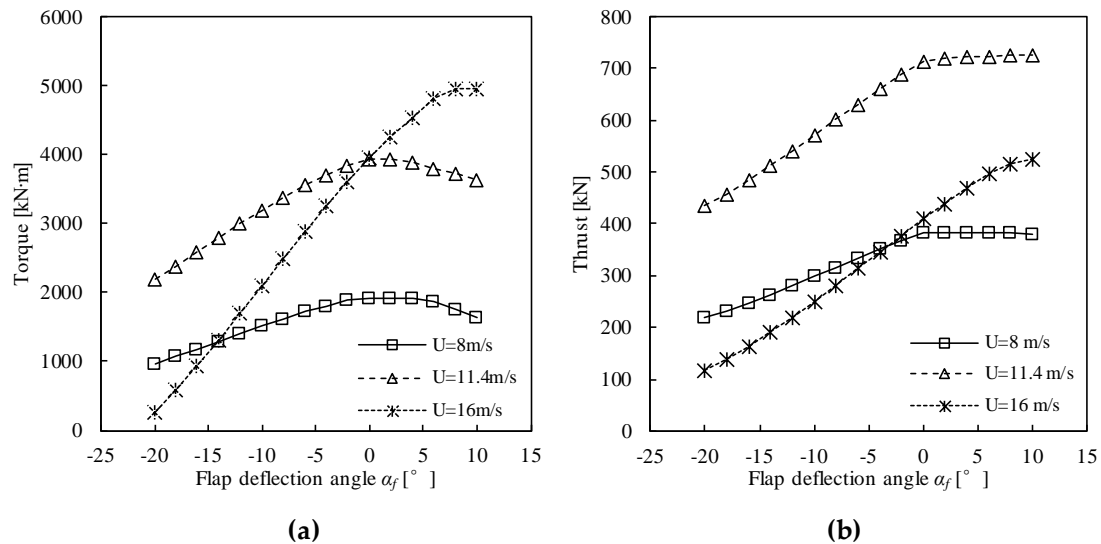


Figure 5. Effect of the trailing-edge flap deflection angle on the torque and thrust of the NREL 5-MW wind turbine rotor. (a) Low speed shaft torque, (b) Rotor thrust.

The FVW model simplifies the blade surface load to a series of centralized loads at the blade element control points. By analyzing the changes in the centralized loads, the influence of the flap deflection on the blade aerodynamic load distribution can be determined. Figures 6–8 show the aerodynamic load distributions of the blade control points at three wind speeds of 8 m/s, 11.4 m/s, and 16 m/s, respectively. It is evident that the curves exhibit a similar trend at 8 m/s and 11.4 m/s although the values in the two figures are different. At wind speeds of 8 m/s and 11.4 m/s, the tangential and normal forces of the tip flaps increase with the increase in the flap deflection angle. The deflection of flap only has a significant effect especially on the loads that are generated in the radial distribution of the flaps, but has little effect on the other position of the blade. It is worth noting that when the deflection angle of the flaps is equal to 5°, the tangential force of the flaps increases slightly and the normal force of the flaps increases considerably. However, the tangential force and the normal force of the other parts decrease slightly. When the wind speed is 16 m/s, the flap deflection also causes significant changes in the tangential force and normal force of the blade tip flaps and also has a considerable impact on the forces at the position near the flaps. The influence range is more than 20% of the blade length. A comparison of Figures 6–8 indicates that the smaller the angle of attack of the profile, the greater the change in the blade’s aerodynamic force is when the flap deflection angle changes.

These results indicate that the adjustability of the trailing-edge flap is directly related to the angle of attack of the profile and when the wind speed is less than the rated wind speed of 11.4 m/s, the angle of attack of the profile is larger and there is little change. Therefore, in order to analyze the effect of the flap deflection on the operation of the wind turbine, only the wind speeds of 11.4 m/s and 16 m/s wind speeds (high angle of attack and small angle of attack) need to be considered.

Figures 9 and 10 show the distribution of the axial wind speed in the front and the back of the rotor of the wind turbine with a trailing-edge flap at 11.4 m/s, and 16 m/s, respectively, as determined by the FVW method. The deflection of the flaps has had little effect on the structure of the wake flow field, but still changes the axial velocity distribution near the blade. At a wind speed of 11.4 m/s, the axial velocity of the front and rear blades increases significantly with the decrease in the flap deflection angle, especially at the tip flaps. In contrast, the wind speed in the low wind speed region of the tip

vortex is increasing. At a wind speed of 16 m/s, the distance between the tip vortices is larger and the decrease in the axial wind speed at the tip vortices does not change significantly with a change in the deflection angle of the flaps. As the flap deflection angle decreases, the change in the distribution of the axial wind speed at the tip flaps becomes more apparent but the change in the other parts of the blades is not significant.

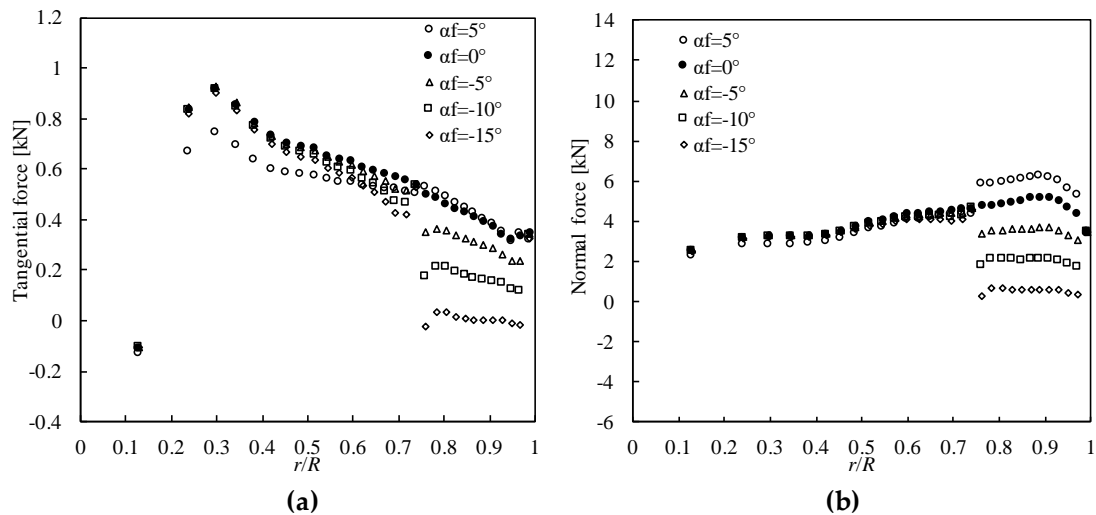


Figure 6. Aerodynamic force distribution of the blade control points for $U = 8$ m/s. (a) Tangential force to the rotor disc, (b) Normal force to the rotor disc.

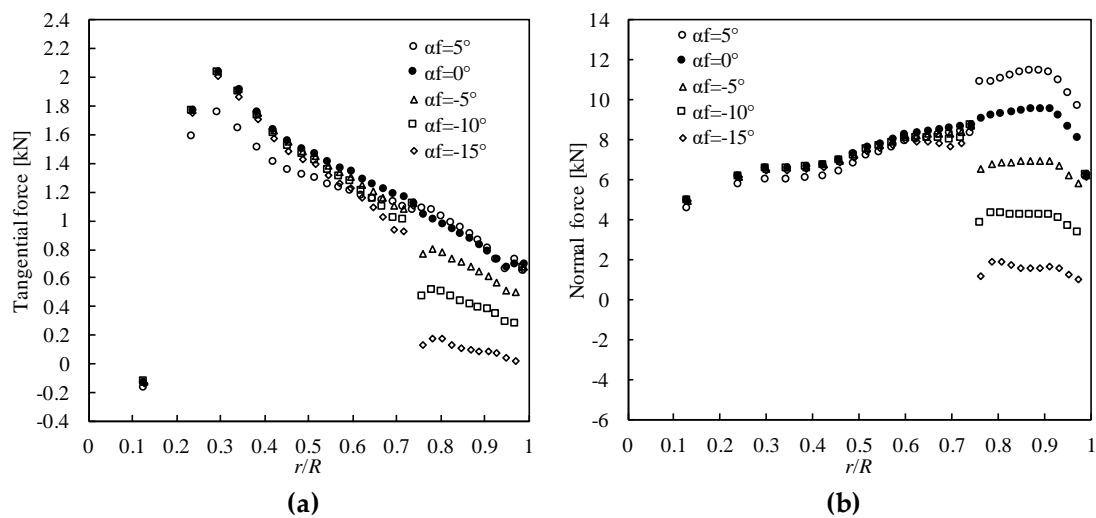


Figure 7. Aerodynamic force distribution of the blade control points for $U = 11.4$ m/s. (a) Tangential force to the rotor disc, (b) Normal force to the rotor disc.

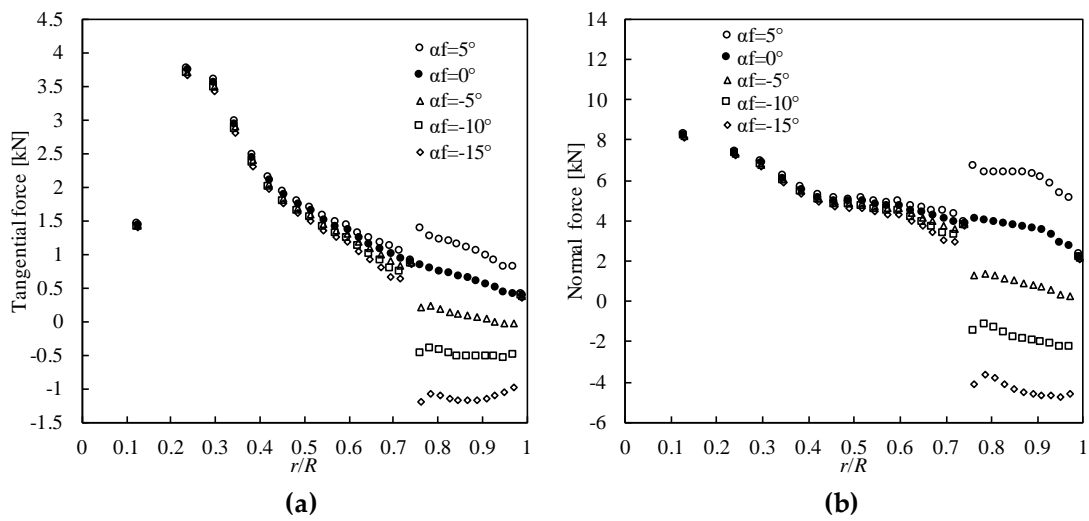


Figure 8. Aerodynamic force distribution of the blade control points for $U = 16$ m/s. (a) Tangential force to the rotor disc, (b) Normal force to the rotor disc.

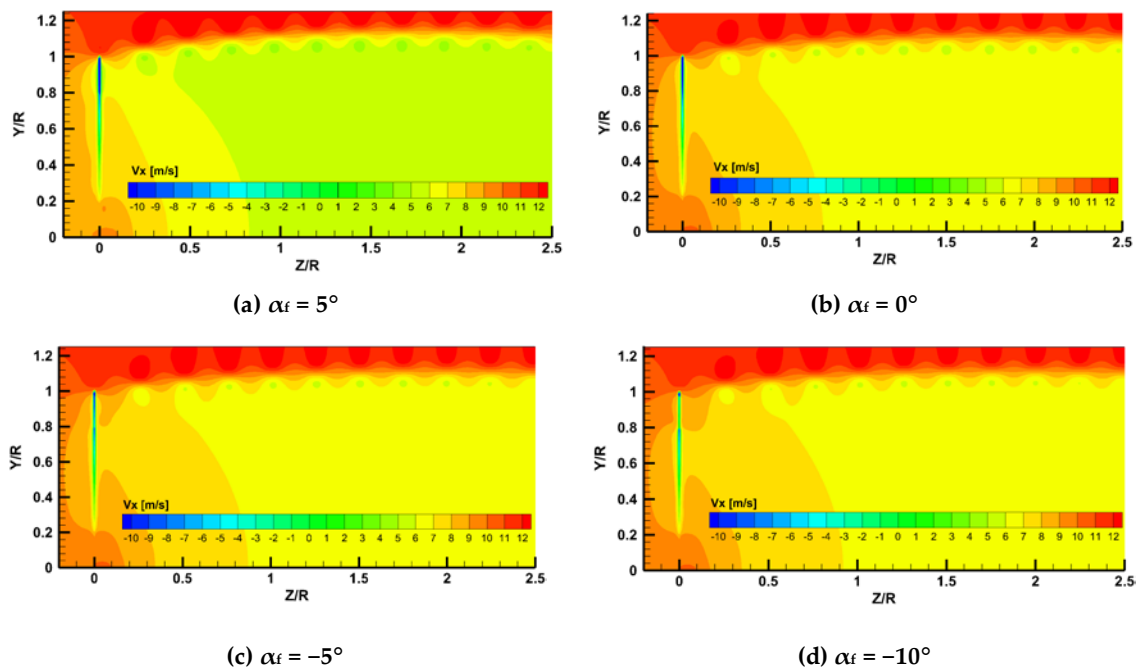


Figure 9. Axial velocity distribution on the plane with a 0° wake angle for $U = 11.4$ m/s. (Position: Axial direction from $-0.2 R$ to $3 R$, radial direction from 0 to $1.25 R$). (a) $\alpha_f = 5^\circ$, (b) $\alpha_f = 0^\circ$, (c) $\alpha_f = -5^\circ$, (d) $\alpha_f = -10^\circ$.

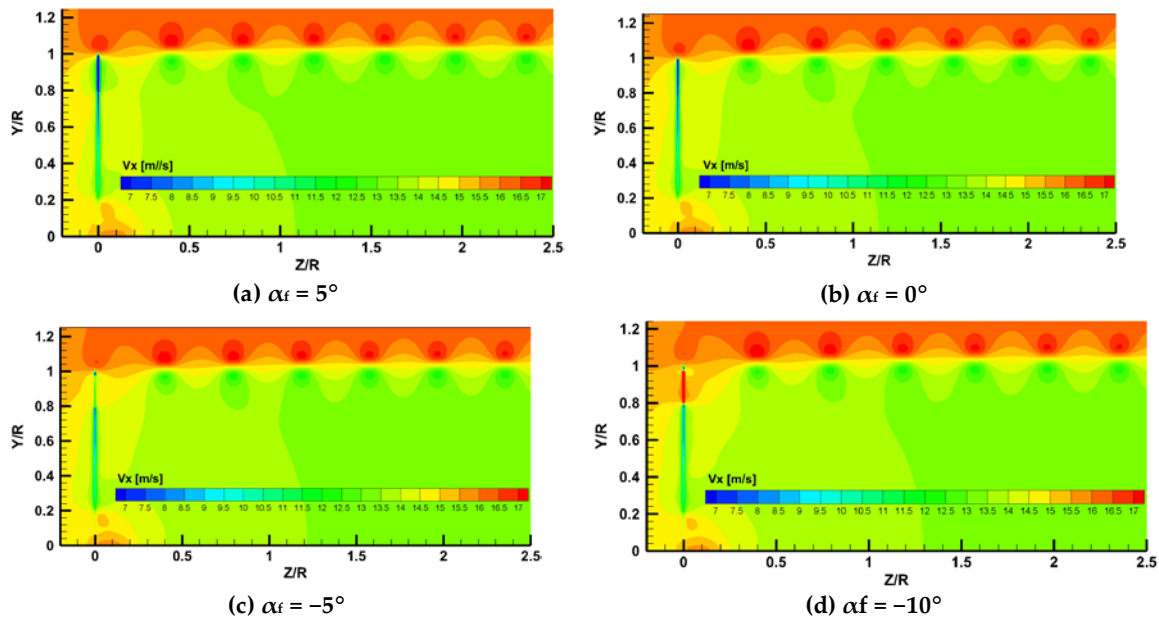


Figure 10. Axial velocity distribution on the plane with a 0° wake angle for $U = 16$ m/s. (Position: Axial direction from $-0.2 R$ to $3 R$, radial direction from 0 to $1.25 R$). (a) $\alpha_f = 5^\circ$, (b) $\alpha_f = 0^\circ$, (c) $\alpha_f = -5^\circ$, (d) $\alpha_f = -10^\circ$.

5. Unsteady Wind Conditions

The trailing-edge flap is used to control the load fluctuation caused by unsteady wind conditions. The unsteady wind field of the wind turbines near the ground mainly includes wind shear and turbulent wind.

5.1. Wind Shear

Wind shear exists in the atmosphere near the ground and is affected by the thickness of the surface boundary layer. Common wind shear models are the exponential model and logarithmic model [25]. Here we choose the exponential model because the prediction of the exponential model agrees better with the measured value than that of the logarithmic model. The boundary layer wind speed is defined as,

$$U(h) = U(h_0) \left(\frac{h}{h_{hub}} \right)^\alpha \tag{2}$$

where $U(h)$ is the wind speed at a height of h and $U(h_0)$ is the wind speed at the reference height h_{hub} . The power law exponent α is usually in the range of $0.1-0.25$. Figure 11 shows the wind shear distribution near the ground where the wind turbine is located. Generally, 0.2 is used on land and 0.1 is used over the ocean [26]. In this study, 0.1 is used.

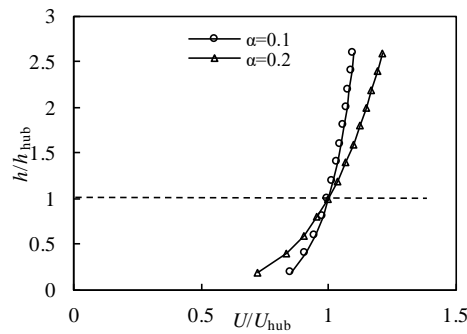


Figure 11. Atmospheric boundary layer profiles.

5.2. Turbulent Wind

Turbulent wind has a complex spatial distribution and in actual wind data, the turbulent intensity is rarely uniform. Therefore, we use the Blade 4.3 software [27] to generate turbulent wind data. The wavelet inverse transformation method [28] is used to create the turbulent wind field according to the advanced von Karman power density spectrum [27]. The surface roughness is 0.01 and the turbulent intensity is 9.58%. Figure 12a,b shows the data of the axial turbulent wind speed at the hub of the wind turbine at wind speeds of 11.4 m/s, and 16 m/s, respectively. Turbulent wind is unevenly distributed in the plane of the wind turbine but it is difficult to quickly measure the wind speed at different coordinate points and analyze the data using existing wind turbine measuring equipment. Therefore, the wind speed data at the hub should be simplified to determine the wind speed change in the entire plane of the wind turbine.

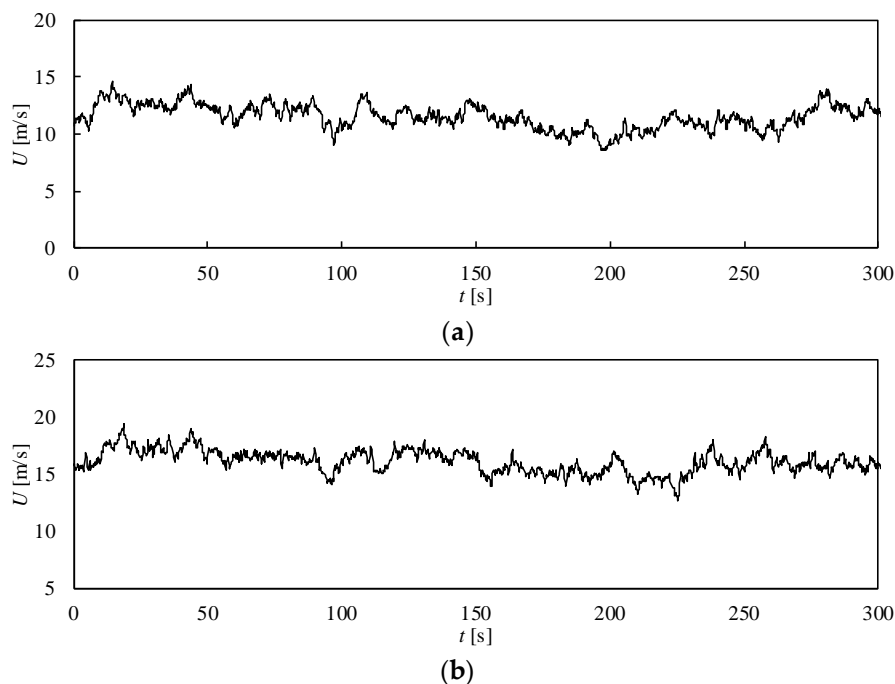


Figure 12. Axial velocities in turbulent conditions with a turbulence intensity of 9.58%. (a) The average wind velocity equals 11.4 m/s; (b) the average wind velocity equals 16 m/s.

6. The Trailing-Edge Flap Control Strategy

In Sections 3 and 4, the influence of the flaps on the aerodynamic load and wake flow field of the wind turbine was analyzed. The control performance of the flaps is related not only to the aerodynamic

characteristics of the flaps but also to the control of the flaps. Here we adopt the flap control strategy proposed by Xu et al. [17]. This method is simple and efficient.

Under wind shear, the minimum wind speed occurs at the lowest point of the wind turbine ($\psi = 90^\circ$) and the maximum wind speed occurs at the highest point of the wind turbine ($\psi = 270^\circ$). The control of wind shear is based on the azimuth angle of the blades. The three blades of the wind turbine are controlled by three separate control units to deal with the load deviation at their respective locations. The control strategy of a single blade is defined as,

$$\alpha_s(t) = a \cdot \left(\frac{U_{hub} - U_{tip}}{|U_{hub} - U_{min}|} \right) \cdot \left| \frac{U_{hub} - U_{tip}}{|U_{hub} - U_{min}|} \right| \quad (3)$$

where a is the flap control factor of the wind shear, U_{hub} is the wind speed at the hub, U_{min} is the minimum value of U_{tip} , and U_{tip} is the wind speed at the blade tip, which is defined as,

$$U_{tip} = U_{hub} \left(\frac{h_{hub} - R \sin \psi}{h_{hub}} \right)^\alpha \quad (4)$$

where h_{hub} is the height of the hub, R is the blade length, ψ is the blade azimuth angle, and the power law exponent α is the same as in Equation (2).

The control of turbulent wind is based on the average wind speed within one second. Since the sampling period of the turbulent wind speed data in this study is 0.25 s, the control strategy of turbulent wind can be described as follows,

$$\alpha_t(t) = b \cdot (U - U_t) \quad (5)$$

where b is the control factor of the turbulence, U is the instantaneous wind speed, U_t is the average wind speed within one second prior to the time, which is expressed as.

$$U_t = \frac{u_t + u_{t-0.25} + u_{t-0.5} + u_{t-0.75} + u_{t-1}}{5} \quad (6)$$

where u_t is the wind speed at current time, $u_{t-0.25}$, $u_{t-0.5}$, $u_{t-0.75}$ and u_{t-1} are the wind speed at times of 0.25 s, 0.5 s, 0.75 s, and 1 s before u_t .

The control factors a and b are essential to the effect of load mitigation and are dependent on the design of the wind turbine [17]. The control strategy engineers need to go through lots of debugging to obtain the appropriate values. In the following, the influence of value changes of factors a and b will be analyzed and the specific values for the NREL 5-MW wind turbine will be proposed.

7. Result and Discussion

7.1. Calculation Results of Wind Shear

Figure 11 shows that there are considerable differences in the wind speed in the vertical direction when the wind turbine tower is high and the blades are long. Figure 13 shows the tangential and normal forces at the control points for different blade azimuths on the NREL 5-MW wind turbine blades under wind shear with a hub wind speed of 11.4 m/s. It is evident that the aerodynamic load is considerably different for different blade azimuths due to the presence of wind shear. For every rotation cycle of the blade, this load change causes fluctuations in the blade's torque and thrust. The force change with the azimuth angle at the outer part of the blade, except the blade tip, which is mainly focused on noise abatement, appears more obvious than at the inner part.

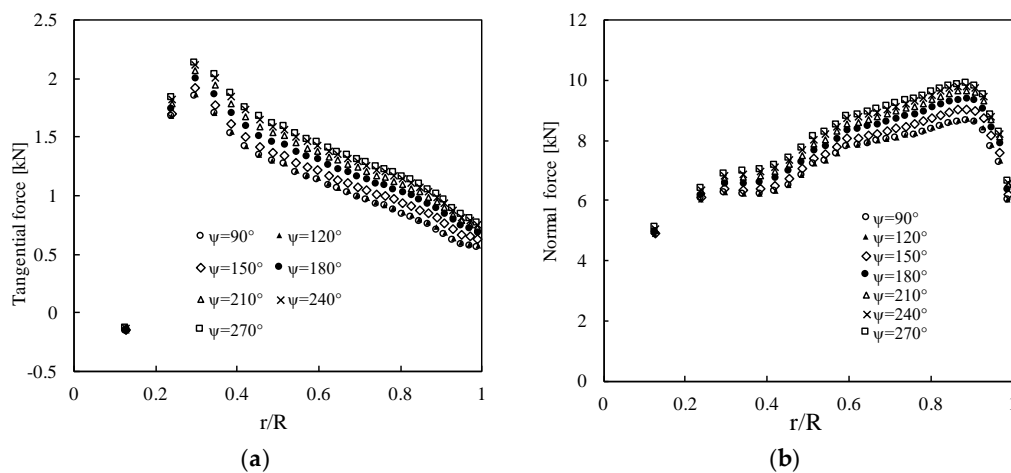


Figure 13. Tangential force and normal force at the control points in wind shear conditions. (a) Tangential force; (b) Normal force.

Figure 14 shows the results of different control factors under wind shear for $U_{hub} = 11.4$ m/s. The results of $a = 0$ are these which were conducted without using control strategies but at a constant flap angle of 0° . Although, the analysis of the blade’s aerodynamic load distribution shows that wind shear has a large influence on the load distribution of the blades, it is observed in Figure 14 that the fluctuations of the torque and thrust ($a = 0$) of the rotor are not very large and are mainly attributed to the superposition of the three blades of the rotor. The torque and thrust ($a = 0$) fluctuations of a single blade are relatively large as shown in Figure 15.

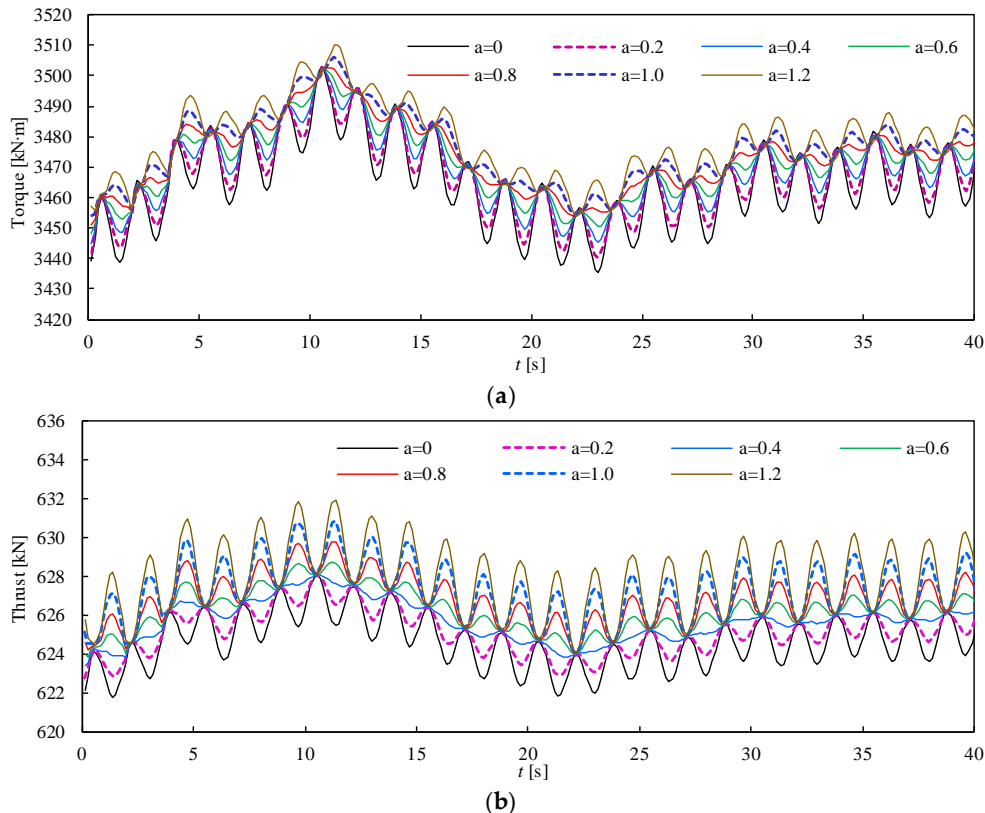


Figure 14. Torque and thrust response of the wind turbine rotor under wind shear conditions for $U_{hub} = 11.4$ m/s. (a) Torque response; (b) thrust response.

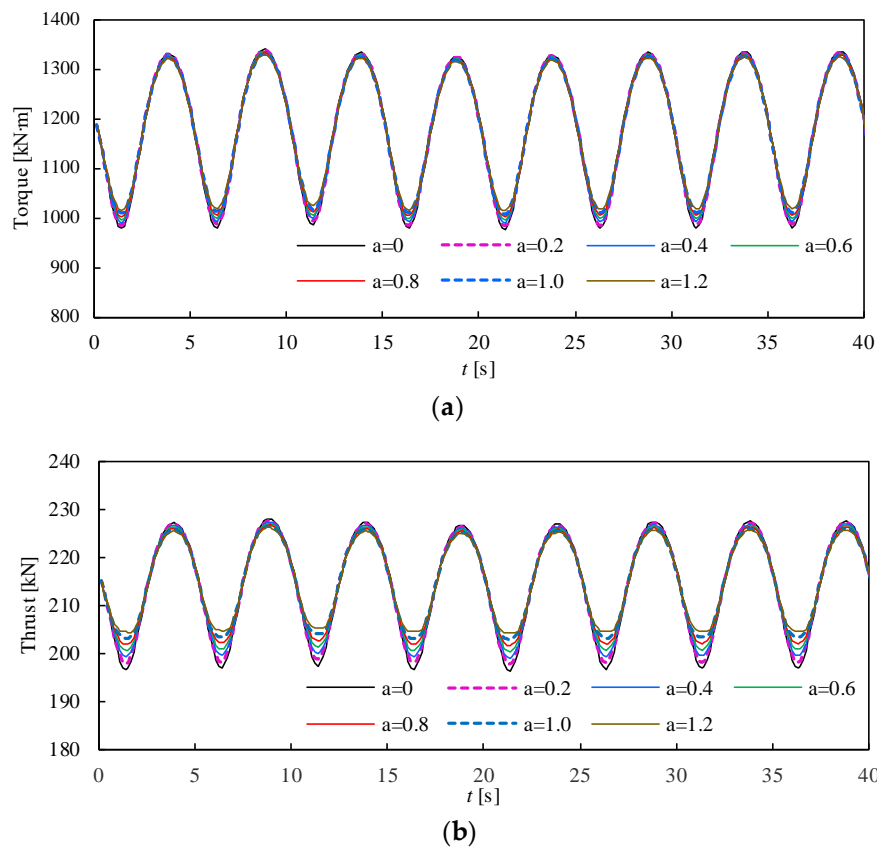


Figure 15. Torque and thrust response of a single blade under wind shear conditions for $U_{\text{hub}} = 11.4$ m/s. (a) Torque response; (b) thrust response.

Different values of the control factors also have different effects. As shown in Figure 14, a change in the value of the flap control factor a significantly changes the amplitude of the torque and power fluctuations. It is noteworthy that the torque curve of the wind turbine has the smallest fluctuation range at $a = 0.8$ but the adjustment of the thrust has overshoot under this condition; the thrust curve has the smallest fluctuation range at $a = 0.4$. Whereas, the torque fluctuation is large at this value. Figure 15 shows that under this wind condition, the effect of the flaps on the torque fluctuation of a single blade is considerably less than that on the thrust fluctuation and the effect on the curve’s crest is less than that on the trough. This is also the reason why the optimal control factors (a) of the torque and thrust of the wind turbine are different under this condition.

When the wind speed is higher than the rated wind speed, the control system limits an additional increase in the power of the wind turbine by increasing the pitch angle. Increasing the pitch angle will reduce the blade’s aerodynamic angle of attack and the aerodynamic characteristics of the flaps (Section 4) show that the flaps with a smaller angle of attack have a larger and more stable adjustment range, which improves the ability of the trailing-edge flaps to control the load.

Because the origin of the flap’s deflection angle is -5° , the torque and thrust of the wind turbine will be significantly less than the original thrust and torque of the NREL 5-MW wind turbine at high wind speeds. When the wind speed is greater than 11.4 m/s, the original pitch angle should be reduced by one unit in order to maintain the wind turbine power stable at around 5 MW, which is a necessary operation in the pitch control system after the trailing-edge flaps are installed. The results at $U_{\text{hub}} = 16$ m/s are calculated to observe the effect of the controller at a small angle of attack of the flap. A number of tests and data analyses indicate that modifying the original pitch angle of 12.06° to 10.5° ensures that the power of the wind turbine can be maintained at around 5 MW. The result is shown in Figure 16. It is observed that the torque and thrust responses are synchronous. When $a = 0.6$, the

fluctuations of the thrust curve and torque curve are very small. Compared with Figure 15, high wind speed and small angle of attack are suitable when using trailing-edge flaps.

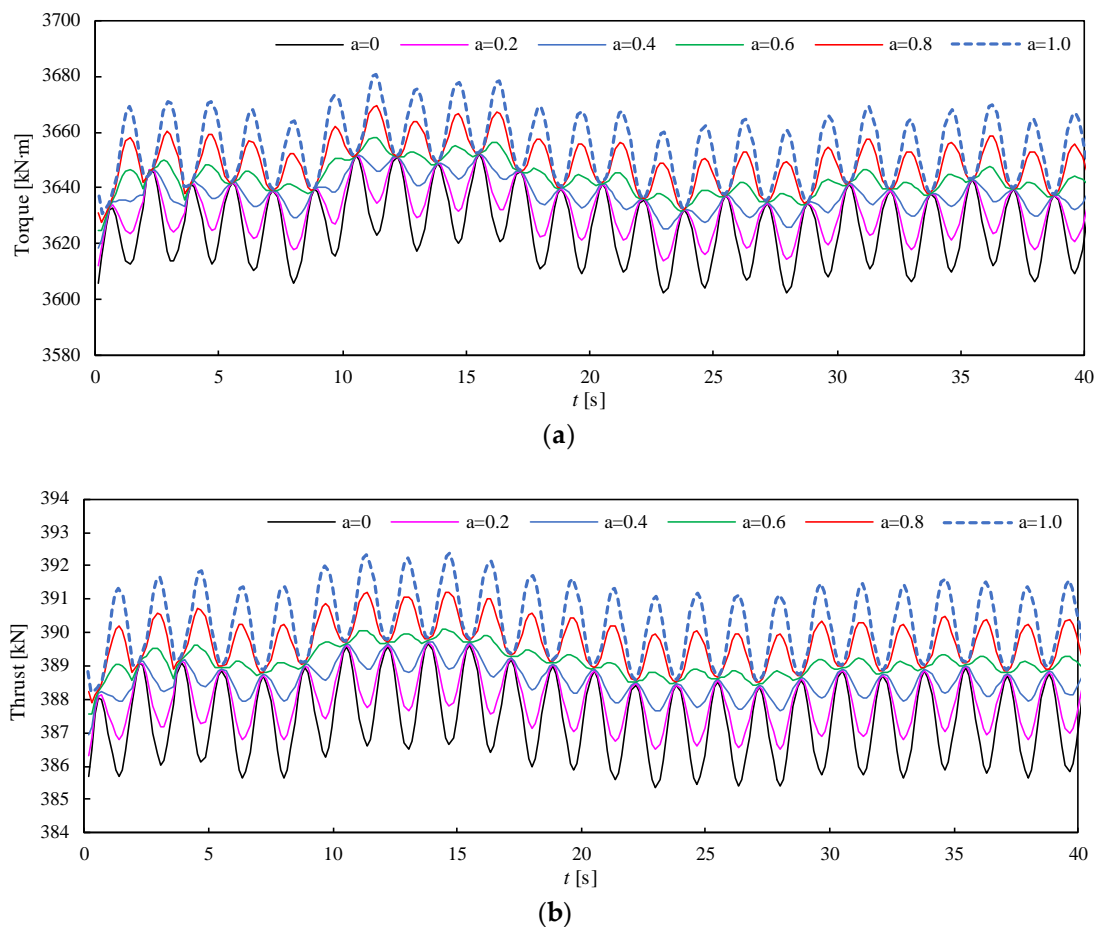
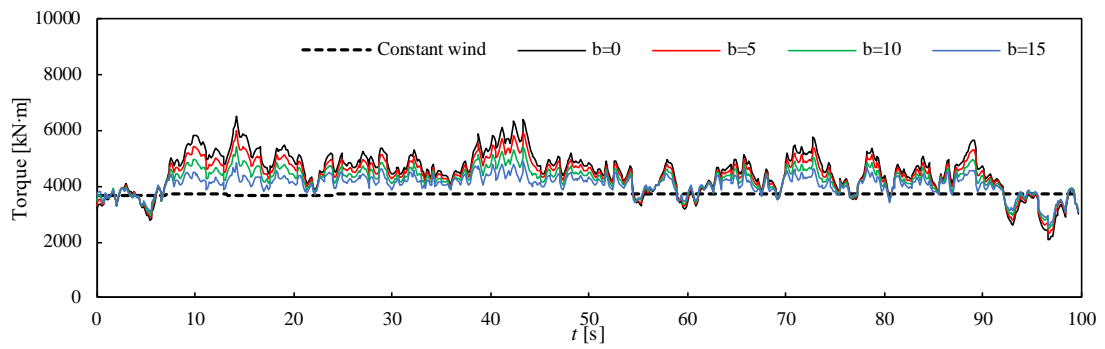


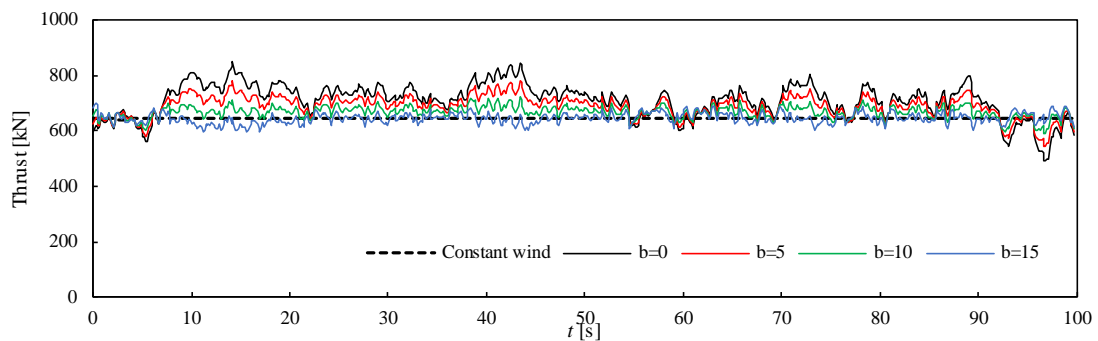
Figure 16. Torque and thrust response of the wind turbine rotor under wind shear conditions for $U_{hub} = 16$ m/s and $\theta_p = 10.5$. (a) Torque response; (b) Thrust response.

7.2. Calculation Results of Turbulent Wind

The performance of the flaps under turbulent wind conditions is an important index to test their load mitigation ability. Figure 17 shows the thrust and torque responses for $U_{mean} = 11.4$ m/s and Figure 18 shows the thrust and torque responses for $U_{mean} = 16$ m/s. The simulation time is 200 s. For the convenience of observation, the figures show the first 100 s. The value range of b is 0–15. The results of $b = 0$ are these which were conducted without using control strategies but at a constant flap angle of 0° . It is evident that an appropriate control factor can mitigate the load fluctuations of the wind turbine, especially for low-frequency fluctuations. For high-frequency fluctuations near the average value, the effect is very small. As shown in Figure 17, when b equals the maximum value of 15, the thrust curve fluctuates in a small range above and below the constant wind curve, while there is a small deviation between the torque curve and the constant curve. At the same turbulence intensity, the turbulence fluctuation amplitude at the average wind speed of 16 m/s is larger than that at the average wind speed of 11.4 m/s. Therefore, the amplitudes of the torque and thrust are larger at 16 m/s than at 11.4 m/s and the performance of the flap is better for the same control factor (see Figure 18). When b equals the maximum value of 15, the torque curves and thrust curves remain near the average value and their amplitudes remain low. This is in agreement with our finding that the trailing-edge flap performs better at high wind speeds and a small angle of attack.

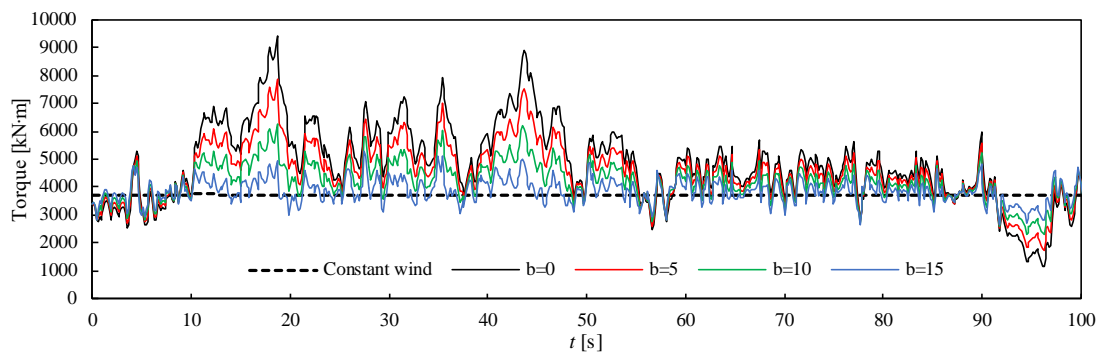


(a)

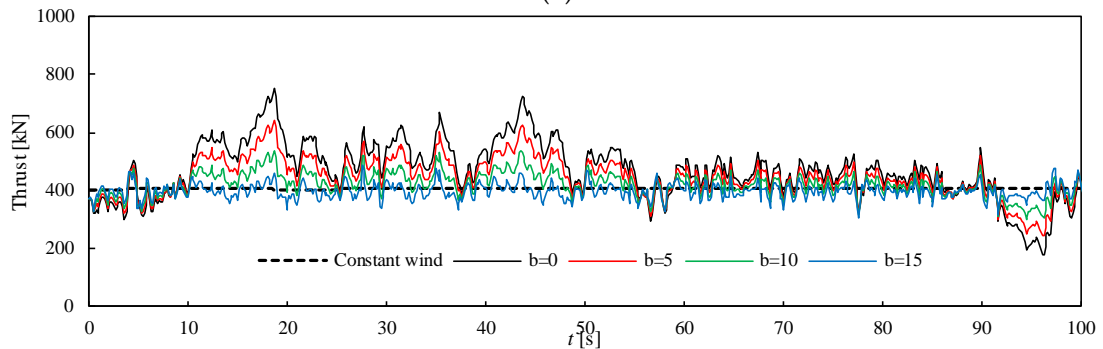


(b)

Figure 17. Torque and thrust response of the wind turbine rotor under turbulent wind conditions for $U_{\text{mean}} = 11.4$ m/s. (a) Torque response; (b) thrust response.



(a)



(b)

Figure 18. Torque and thrust response of the wind turbine rotor under turbulent wind conditions for $U_{\text{mean}} = 16$ m/s and $\theta_p = 10.5^\circ$. (a) Torque response; (b) thrust response.

8. Conclusions

In this study, the effect of a trailing-edge flap on load mitigation in a large-scale offshore NREL 5-MW wind turbine was analyzed by using the FVW model.

Firstly, the variation of airfoil aerodynamic performance due to the trailing edge flap deflection is obvious. The deflection of flap has a significant effect especially on the loads that are generated in the radial distribution of the flaps. The smaller the angle of attack of the profile, the greater the change in the blade's aerodynamic force is when the flap deflection angle changes. Besides, the deflection of flap has a significant effect on the axial velocity of wake especially in the near wake of the outer part of the blade.

Secondly, control strategies of the trailing-edge flap for the shear wind and turbulent wind conditions were developed. The application of the trailing-edge flap control strategy can mitigate the fluctuation of load (torque and thrust) well in above unsteady conditions. The proposed control factor values of $a = 0.6$ and $b = 15$ were obtained for the NREL 5-MW wind turbine.

In a word, the control factors a and b are essential to the effect of load mitigation and are dependent on the design of the wind turbine. Some practical applications will be conducted in the future.

Author Contributions: Conceptualization, X.C. and Y.W.; methodology, B.X.; software, Y.W.; validation, X.C., Y.W., B.X. and J.F.; formal analysis, B.X.; investigation, X.C. and Y.W.; resources, X.C.; data curation, J.F.; writing—original draft preparation, Y.W. and J.F.; writing—review and editing, B.X.; visualization, Y.W.; supervision, X.C.; project administration, X.C.; funding acquisition, X.C. and B.X. All authors have read and agreed to the published version of the manuscript.

Funding: This research was funded by the Fundamental Research Funds for the Central Universities (grant number 2018B48614, 2019B14614); and the National Natural Science Foundation of China (grant number 51607058).

Conflicts of Interest: The authors declare no conflict of interest.

References

- Li, Y.; Le, C.; Ding, H.; Zhang, P.; Zhang, J. Dynamic Response for a Submerged Floating Offshore Wind Turbine with Different Mooring Configurations. *J. Mar. Sci. Eng.* **2019**, *7*, 115. [[CrossRef](#)]
- Loth, E.; Steele, A.; Qin, C.; Ichter, B.; Selig, M.S.; Moriarty, P. Downwind pre-aligned rotors for extreme-scale wind turbines. *Wind Energy* **2017**, *20*, 1241–1259. [[CrossRef](#)]
- Vamsi, I.; Sabareesh, G.R.; Penumakala, P.K. Comparison of condition monitoring techniques is assessing fault severity for a wind turbine gearbox under non-stationary loading. *Mech. Syst. Signal Process.* **2019**, *124*, 1–20. [[CrossRef](#)]
- Barlas, T.K.; van Kuik, G.A.M. Review of state of the art in smart rotor control research for wind turbines. *Prog. Aerosp. Sci.* **2010**, *46*, 1–27. [[CrossRef](#)]
- Li, M.; He, Y.L.; Li, C.W. Study and analysis on collaborated control simulation for the new typed transmission system of wind turbine set. *J. Mach. Des.* **2008**, *25*, 36–40.
- Cheng, Y.; Xue, Z.; Jiang, T.; Wang, W.; Wang, Y. Numerical simulation on dynamic response of flexible multi-body tower blade coupling in large wind turbine. *Energy* **2018**, *152*, 601–612. [[CrossRef](#)]
- Xia, Y.; Sun, D.Y. Characteristic analysis on a new hydro-mechanical continuously variable transmission system. *Mech. Mach. Theory* **2018**, *126*, 457–467. [[CrossRef](#)]
- Jang, M.H.; Lee, J.H.; Chung, Y.D. A study of a hydraulic torque converter for the offshore wind turbine system. In Proceedings of the International Conference on Electrical Machines and Systems, Busan, Korea, 26–29 October 2013; pp. 2305–2308.
- Chopra, I. Review of state of art of smart structures and integrated systems. *AIAA J.* **2002**, *40*, 2145–2187. [[CrossRef](#)]
- Hansen, M.O.; Madsen, H.A. Review paper on wind turbine aerodynamics. *J. Fluids Eng.* **2011**, *133*, 114001. [[CrossRef](#)]
- Chen, H.; Qin, N. Trailing-edge flow control for wind turbine performance and load control. *Renew. Energy* **2017**, *105*, 419–435. [[CrossRef](#)]
- Roget, B.; Chopra, I. Wind-tunnel testing of rotor with individually controlled trailing-edge flaps for vibration reduction. *J. Aircr.* **2008**, *45*, 868–879. [[CrossRef](#)]

13. Bak, C.; Gaunaa, M.; Andersen, P.B.; Buhl, T.; Hansen, P.; Clemmensen, K. Wind tunnel test on airfoil Risø-B1-18 with an Active Trailing Edge Flap. *Wind Energy* **2010**, *13*, 207–219. [[CrossRef](#)]
14. Lee, T.; Su, Y.Y. Lift enhancement and flow structure of airfoil with joint trailing-edge flap and Gurney flap. *Exp. Fluids* **2011**, *50*, 1671–1684. [[CrossRef](#)]
15. Lu, W.S.; Tian, Y.; Liu, P.Q. Aerodynamic optimization and mechanism design of flexible variable camber trailing-edge flap. *Chin. J. Aeronaut.* **2017**, *30*, 988–1003. [[CrossRef](#)]
16. Lackner, M.A.; Kuik, G.V. A comparison of smart rotor control approaches using trailing edge flaps and individual pitch control. *Wind Energy* **2010**, *13*, 117–134. [[CrossRef](#)]
17. Xu, B.F.; Feng, J.H.; Wang, T.G.; Yuan, Y.; Zhao, Z.Z.; Zhong, W. Trailing-edge flap control for mitigating rotor power fluctuations of a large-scale offshore floating wind turbine under the turbulent wind condition. *Entropy* **2018**, *20*, 676. [[CrossRef](#)]
18. Xu, B.F.; Wang, T.G.; Yuan, Y.; Cao, J.F. Unsteady aerodynamic analysis for offshore floating wind turbines under different wind conditions. *Philos. Trans. R. Soc. A Math. Phys. Eng. Sci.* **2015**, *373*. [[CrossRef](#)]
19. Sabale, A.; Gopal, N. Nonlinear aeroelastic analysis of large wind turbines under turbulent wind conditions. *AIAA J.* **2019**, *57*, 4416–4432. [[CrossRef](#)]
20. Weissinger, J. The lift distribution of swept-back wings. In *Technical Report NACA-TM-1120*; National Advisory Committee for Aeronautics: Washington, DC, USA, 1947.
21. Xu, B.F.; Wang, T.G.; Yuan, Y.; Zhao, Z.Z.; Liu, H.M. A simplified free vortex wake model of wind turbines for axial steady conditions. *Appl. Sci.* **2018**, *8*, 866. [[CrossRef](#)]
22. Jonkman, J.; Butterfield, S.; Musial, W.; Scott, G. *Definition of a 5 mw Reference Wind Turbine for Offshore System Development*; Office of Scientific & Technical Information Technical Reports; National Renewable Energy Lab. (NREL): Golden, CO, USA, 2009.
23. Xu, B.F.; Feng, J.H.; Xu, C.; Zhao, Z.Z.; Yuan, Y. Aerodynamic performance analysis of a trailing-edge flap for wind turbines. *J. Phys. Conf. Ser.* **2018**, *1037*, 022020.
24. Zhang, W.G.; Wang, Y.F.; Liu, R.J. Unsteady aerodynamic modeling and control of the wind turbine with trailing edge flap. *J. Renew. Sustain. Energy* **2018**, *20*, 063304. [[CrossRef](#)]
25. Large, W.G.; McWilliams, J.C.; Doney, S.C. Oceanic vertical mixing: A review and a model with a nonlocal boundary layer parameterization. *Rev. Geophys.* **1994**, *32*, 363. [[CrossRef](#)]
26. Khosravi, M.; Sarkar, P.; Hu, H. An experimental investigation on the performance and the wake characteristics of a wind turbine subjected to surge motion. *AIAA J.* **2016**, *138*, 042602.
27. Bossanyi, E.A. *GH Bladed Theory Manual*; Garrad Hassan and Partners Ltd.: Bristol, UK, 2009.
28. Kitagawa, T.; Nomura, T. A wavelet-based method to generate artificial wind fluctuation data. *J. Wind Eng.* **2003**, *91*, 943–964. [[CrossRef](#)]



© 2020 by the authors. Licensee MDPI, Basel, Switzerland. This article is an open access article distributed under the terms and conditions of the Creative Commons Attribution (CC BY) license (<http://creativecommons.org/licenses/by/4.0/>).